Journal of Modern Optics
Vol. 52, No. 9, 15 June 2005, 1243–1253

Taylor & Francis
Taylor & Francis Group

Femtosecond resonance enhanced CARS for background-free detection of organic molecules

ALEKSANDER REBANE*†, MIKHAIL DROBIZHEV‡, MIKALAI KRUK§, ALIAKSANDR KAROTKI†, IMBI TEHVER¶ and MARLAN SCULLY‖

†Department of Physics, Montana State University, Bozeman, MT 59717, USA
‡Permanent address: Lebedev Physics Institute, Leninsky pr., 53, 119991 Moscow, Russia
§Institute of Molecular and Atomic Physics, 220072 Minsk, Belarus
¶Institute of Physics, Tartu University, Riia 142, Tartu 51014, Estonia
‖Department of Physics, Texas A & M University, College Station, TX 77843-4242, USA

(*Received 8 May 2004; in final form 21 October 2004*)

We study the coherent excitation profile (CEP) of resonance enhanced femtosecond CARS in a model system zinc phthalocyanine in a polymer film host as a prospective technique for detection and identification of molecular species in ambient environments. A new method of suppressing the non-resonant FWM background is demonstrated. Transform theory is applied to calculate CEP based on the absorption spectrum, and good agreement between theory and experiment is obtained.

1. Introduction

Recently there has been increased interest in using advanced techniques of ultrafast laser excitation, in particular coherent anti-Stokes Raman scattering (CARS), as a tool for real-time detection of molecular and biological agents, including airborne contaminants such as bacterial spores [1, 2]. The potential high selectivity of the proposed technique is based on the fact that the CARS signal can be sensitive both to the electronic and vibrational signature of the species under investigation. On the other hand, excitation with high intensity ultrashort (femtosecond) pulses can bring about high optical gain, and associated high brightness of the CARS signal, which offers prospects of high sensitivity and high selectivity of detection.

The studies performed so far on ultrafast CARS in organic systems have emphasized separation and recognition of individual vibrational modes [3–5]. In the case of biologically relevant species, which are typically characterized by a large number of vibrational and electronic degrees of freedom, such separation of

*Corresponding author. Email: rebane@physics.montana.edu

Journal of Modern Optics
ISSN 0950–0340 print/ISSN 1362–3044 online © 2005 Taylor & Francis Group Ltd
http://www.tandf.co.uk/journals
DOI: 10.1080/09500340512331329091

individual vibrational frequencies becomes rather challenging, both from the view point of implementation, as well as from the view point of interpretation of the results. Furthermore, these measurements rely on polarization to discriminate spurious background signal [6], and require thus highly controlled conditions, such as non-scattering, optically transparent samples, etc.

In this paper we make an attempt to address some of the limitations mentioned above. We use a model molecular system, zinc phthalocyanine (ZnPc) in a solid host, and measure coherent excitation profile (CEP) of CARS signal with femtosecond pulses. Our approach is to make use of the electronic resonance enhancement effect [7–10], by tuning the frequency of one of the two excitation pulses to the absorption frequency of ZnPc. The resulting strong resonance enhancement allows us, on the one hand, to do away with the polarization-based discrimination, and on the other hand, provides us with a characteristic CEP signature.

To perform quantitative analysis of the experiment, we apply the transform theory [11, 12]. Besides being a convenient calculation tool for obtaining CEP from linear absorption data, the transform theory has the advantage that it takes into account all vibrational modes in both excited and ground electronic state. We also apply the current transform theory to predict the ideal amplitude and phase of the excitation pulses to achieve maximum efficiency of the CARS signal.

2. Theoretical considerations

The underlying idea of the transform theory consists in an intrinsic connection that exists between the amplitude of resonant scattering and the corresponding resonant absorption [13] (see also reviews [14, 15]). Normally, according to the optical theorem [16], the complex amplitude of Rayleigh scattering in an atomic gas medium, and at a frequency close to an absorption line resonance, is directly proportional to the linear susceptibility, $\Phi(\omega)$ of the medium. Since the imaginary part of the complex index of refraction is proportional to the coefficient of absorption, then, by measuring the absorption spectrum, and by applying Kramers–Krönig dispersion relations to calculate the real part of the complex index, one can easily find the excitation profile of the resonant Rayleigh scattering. The same approach can be applied to include the excitation profile of spontaneous resonant Raman scattering [13–15, 17, 18], as well as resonant coherent Stokes and anti-Stokes Raman scattering [19–23].

The transform relations for Raman scattering for different types of vibronic coupling were derived in a series of publications (see reviews [15, 17, 24]). The simplest vibronic model, called the basic model, starts out from adiabatic approximation (i.e. the total wave function is the product of an electronic wave function and a vibrational wave function) and Condon approximation (electronic transition matrix element is independent of the vibrational coordinates). This model also assumes that the vibrational potential is harmonic, and that the overlap integral between the vibrational wave functions in the ground and excited electronic states is determined by two identical, but slightly shifted, potentials (linear vibronic coupling model).

In the basic model, the first-order spontaneous complex Raman scattering amplitude, corresponding to one Raman-active vibration, can be expressed as

$$\alpha(\omega_p) = \xi_j[\Phi(\omega_p) - \Phi(\omega_p - \omega_j)], \tag{1}$$

where ω_j is the Raman frequency, ω_p is the excitation laser frequency, and ξ_j denotes the dimensionless Stokes shift of the vibration. The complex refractive index, $\Phi(\omega)$, can be found from the normalized absorption line shape function, $I(\omega)$, by applying Kramers–Krönig dispersion relations

$$\Phi(\omega) = \int_0^\infty \frac{I(\omega')}{\omega' - \omega}\, d\omega' + i\pi I(\omega), \tag{2}$$

where the normalized absorption is defined as

$$I(\omega) = \frac{\sigma(\omega)}{\omega}\left[\int_0^\infty \frac{\sigma(\omega')\, d\omega'}{\omega'}\right]^{-1}, \tag{3}$$

with $\sigma(\omega)$ denoting molecular absorption cross-section.

The third-order nonlinear susceptibility tensor, which is responsible for the resonant CARS process, can be expressed as a product of two simultaneous resonant Raman scattering amplitudes [25]:

$$\chi_{\mathrm{CARS}}(\omega_p) = \alpha_j(\omega_p)\alpha_j(\omega_p + \omega_j). \tag{4}$$

By substituting equation (1) into equation (4), and by considering that the intensity of nonlinear scattering is proportional to the square modulus of the nonlinear susceptibility, we obtain the following CEP if the excitation frequency, ω_p, is varied in the region of the electronic resonance transition:

$$I_{\mathrm{CARS}}(\omega_p) \propto \left|[\Phi(\omega_p) - \Phi(\omega_p - \omega_j)][\Phi(\omega_p + \omega_j) - \Phi(\omega_p)]\right|^2. \tag{5}$$

Note that formula (5) takes into account not only the contribution of the purely electronic resonance transition, but also all transitions involving vibrational modes in the excited electronic state. Because of this property, the current approach is especially well suited to analysis and identification of systems exhibiting a large number of vibrational degrees of freedom, such as macromolecules, solids, and even complex biological agents such as bacterial spores.

If Condon approximation is violated, then we need to take into account the dependence of the electronic transition matrix element on the vibrational coordinates. Accordingly, the Raman scattering amplitude acquires additional terms, known as the Herzberg–Teller interaction. By expanding the electronic matrix element with respect to the vibrational coordinate, Q, and keeping only the first two terms

$$M(Q) = M_0 + M_1 Q, \tag{6}$$

Ref. [26] obtained the following expression for the complex Raman scattering amplitude:

$$\alpha_j(\omega_p) = \xi_j[\Phi(\omega_p) - \Phi(\omega_p - \omega_j)] + M_{1j}[\Phi(\omega_p) + \Phi(\omega_p - \omega_j)]. \tag{7}$$

Substituting equation (7) into equation (5) gives a modified expression for the CEP:

$$\begin{aligned} I_{\mathrm{CARS}}(\omega_p) \propto |\{[\Phi(\omega_p) - \Phi(\omega_p - \omega_j)] + D_j[\Phi(\omega_p) + \Phi(\omega_p - \omega_j)]\} \\ \times \{[\Phi(\omega_p + \omega_j) - \Phi(\omega_p)] + D_j[\Phi(\omega_p + \omega_j) + \Phi(\omega_p)]\}|^2 \end{aligned} \tag{8}$$

where the relative strength of the Herzberg–Teller interaction is accounted for by the parameter, $D_j = M_{1j}/\xi_j$.

3. Experimental

Our experimental arrangement (figure 1) comprised a 1 kHz repetition rate, femtosecond Ti:sapphire regenerative amplifier (Clark MXR, CPA 1000), which was seeded by a mode-locked Ti:sapphire femtosecond oscillator (Coherent, Mira 900) pumped by a cw 5 W power frequency-doubled YAG laser (Coherent Verdi). The regenerative amplifier system produced 0.8 mJ energy, 150 fs duration pulses at wavelength 780 nm. The amplifier output was used as an input of an optical parametric amplifier, OPA (Quantronix, TOPAS), which frequency downconverted the wavelength of the femtosecond pulses to the near-IR range of wavelength. The signal beam output of the OPA was then frequency-doubled in a type I BBO crystal, which resulted in 100 fs duration pulses, with 0.01–0.1 mJ energy and with a wavelength tuning range of about 550–850 nm.

A 5% beamsplitter picked up a small fraction of the amplifier output pulse energy, and was used as the Stokes excitation pulse at a fixed wavelength $\lambda_s = 780$ nm ($\omega_s = 12800\,\mathrm{cm}^{-1}$). The frequency-doubled output of OPA was used as a pump pulse, and was tuned in the wavelength range $\lambda_p = 650$–690 nm ($\omega_p = 15380$–$14500\,\mathrm{cm}^{-1}$). The two excitation beams were adjusted to zero time delay with an optical delay line, and then focused with two separate $f = 20$ cm lenses to a common $d \sim 0.1$ mm diameter spot, at a relative angle $\theta = 3$–5°.

Typical pulse energy was 1–10 μJ in each of the two beams. Both beams were vertically linearly polarized. No special measures were applied to control the polarization. The spectra were measured with a 0.5 m imaging spectrometer equipped with a cooled CCD array detector (JobinYvon, Triax 550 and SpectumOne).

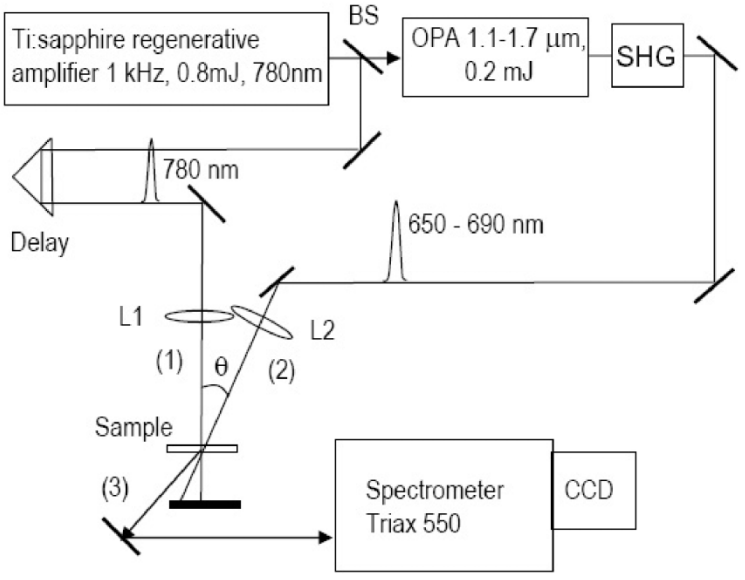

Figure 1. Experimental set-up. BS, 5% beamsplitter; (1) stokes pulse; (2) pump pulse; (3) CARS signal.

The sample was a polyvinylbutyral (PVB) film of thickness, $d = 30\,\mu m$, activated with zinc 2,9,16,23-tetra-tert-butyl-29H,31H-phthalocyanine (ZnPc) at a concentration of 3×10^{-3} mol/litre. A neat PVB film of the same 30 μm thickness was used as a blank comparison sample.

We note that using a constant phase matching angle was justified by the very small thickness of the sample, and by the fact that the maximum phase mismatch that could result from varying the pump frequency under current conditions, $d\,\Delta\omega_p = 3 \times 10^{-3}\,cm \times 880\,cm^{-1} = 2.6$, was sufficiently small, i.e less than π.

4. Results and discussion

The absorption spectrum of the sample in the Q-band region (figure 2) consists of the purely electronic $S_1 \leftarrow S_0$ transition band at 680 nm (14700 cm^{-1}), accompanied at shorter wavelengths by vibronic satellite bands. Characteristic vibrational frequencies in the excited state are in the range up to 2000 cm^{-1}. The insert in figure 2 shows also the spontaneous Raman scattering spectrum of ZnPc, measured under non-resonant 532 nm excitation. This spectrum is similar to that reported for related metal phthalocyanines [27], and exhibits a range of ground state vibrational modes, covering a similar range of frequencies as the absorption spectrum.

In the CARS experiment, the excitation pump frequency is varied in the region of the relatively narrow Q(0–0) absorption resonance. At the same time, the excitation Stokes frequency is considerably below the Q-band, and the Stokes intensity can therefore be considered uniform across the sample. The CARS frequency is generated well above the strongest Q-band, and is only minimally affected by the finite absorption of the sample.

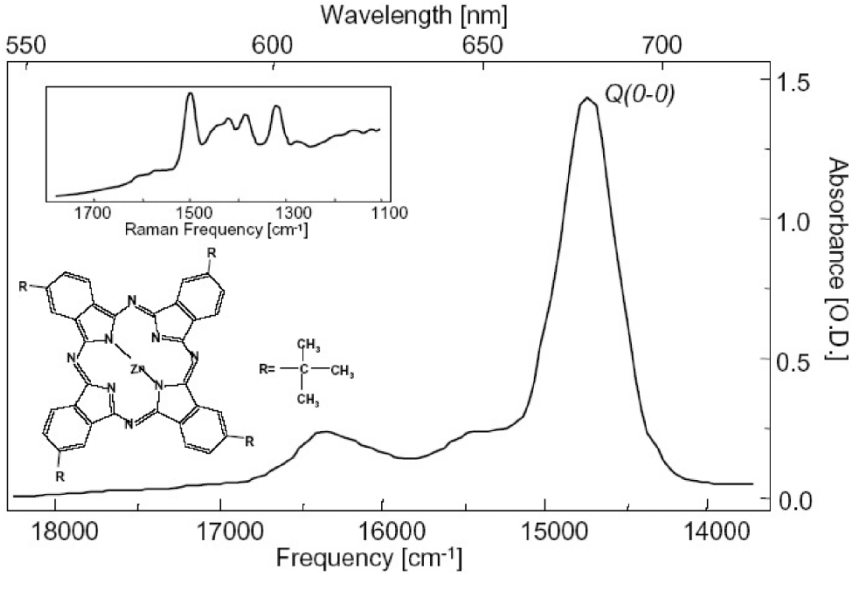

Figure 2. Absorption spectrum of ZnPc sample. Q(0–0) band at 680 nm corresponds to the lowest allowed purely electronic transition. Inserts show Raman scattering spectrum of ZnPc measured with 532 nm laser (boxed) and chemical structure of ZnPc.

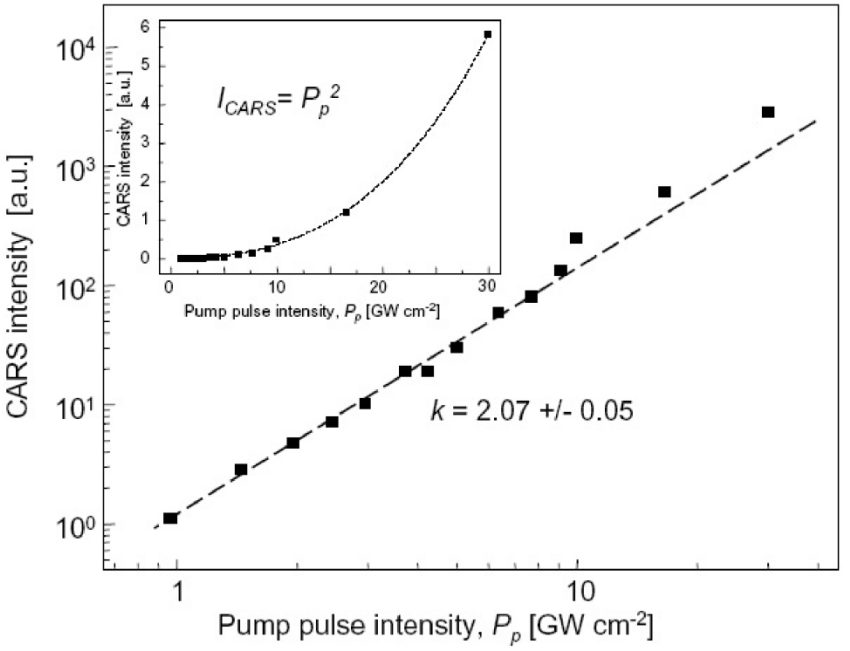

Figure 3. Dependence of CARS signal intensity on the intensity of excitation pump pulse at wavelength $\lambda_p = 650$ nm (rectangles), at constant intensity of Stokes excitation pulse at $\lambda_s = 780$ nm. Dashed line is fit with quadratic function. Insert shows the same data points in linear scale.

Figure 3 shows the measured dependence of the CARS signal intensity on the intensity of the pump pulses. The fact that the dependence follows a quadratic law indicates that, even at the highest pulse intensity, under our experimental conditions the CARS signal was not saturated. In the measurements presented below, the energy of the excitation pulses was maintained in this non-saturated region.

At our experimental conditions, the sample consists predominantly of the host polymer, with the dye molecules making up only 0.1% of the material. Therefore, the measured intensity contains, besides the signal due to ZnPc molecules, also the four wave mixing (FWM) signal arising from the polymer host. Discrimination between the two signals usually achieved by the polarization technique [6, 7], which requires an exact control over the state of polarization of the excitation beams. In our experiment, we took a different approach, which does not rely on the polarization, but rather takes advantage of the resonance enhancement effect. We assembled the ZnPc sample side by side with a blank polymer sample of the same 30 μm thickness. By gradually lowering the intensity of the excitation pulses, with the pump pulse frequency tuned to the 0–0 absorption resonance, and by comparing the signal from two samples under identical excitation conditions, we noticed that the signal from the blank sample decreased more rapidly than that from the sample activated with ZnPc. Below a certain excitation power of about 1–2 GW cm^{-2} only the activated sample gave a detectable signal. Figure 4 shows the measured spectrum from the two samples. We see that under conditions described above, the signal from the ZnPc sample is clearly detectable, whereas that from the pure FWM from the

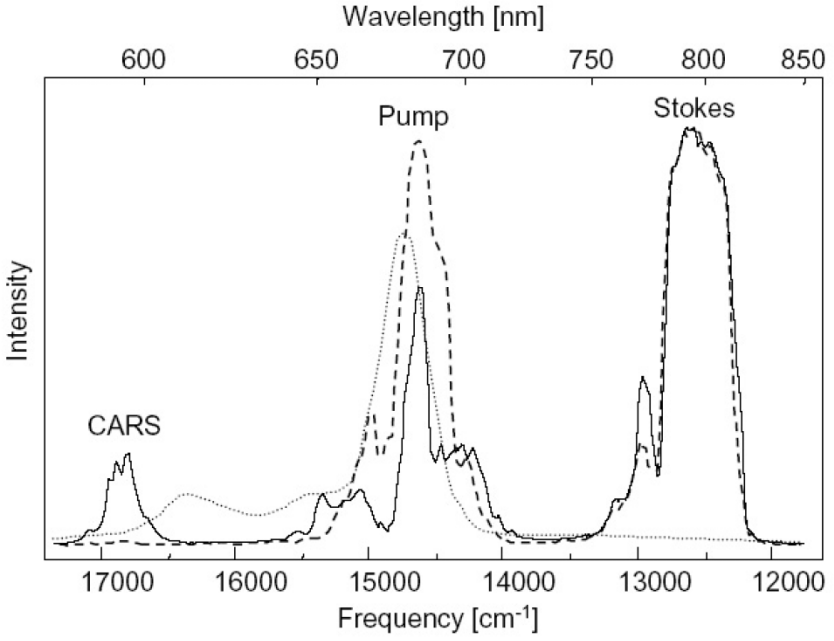

Figure 4. Spectrum of CARS signal in ZnPc-activated sample (——) and in reference blank sample (- - - - -). The spectrum of the pump and Stokes excitation pulses, along with the absorption spectrum of ZnPc (dotted) is shown for comparison.

polymer is practically absent. We explain this difference by increased optical gain at the mixing frequency, $\omega_{\mathrm{CARS}} = 2\omega_{\mathrm{p}} - \omega_{\mathrm{s}}$, in the ZnPc-activated sample, brought about by the electronic resonance condition. From the known relative concentration of the dye molecules (by weight), we estimate that the resonance enhancement increases the CARS efficiency by at least a factor of 10^4. In the following measurements, we took advantage of this property to make sure that the detected signal was predominantly due to the ZnPc molecules, while the FWM background from the host polymer remained negligible small.

The next step in our experiment was to measure the CEP of the CARS signal by varying the pump frequency, while maintaining the stokes frequency as well as the intensity of both illuminating pulses constant. Figure 5 shows that the intensity of the CARS signal increases significantly as ω_{p} approaches the electronic Q(0–0) transition resonance. Note that the maximum of the CEP does not coincide with the absorption maximum, but is rather shifted to lower frequency by about $200\,\mathrm{cm}^{-1}$. In addition, the experiment data indicate that the main CEP maximum is accompanied by some structure on its both sides.

As a trivial explanation, the frequency shift of the CEP maximum could be due to non-uniform intensity of the pump across the sample, especially as the frequency is tuned to the maximum extinction (OD ~ 1.7 at $\lambda = 680\,\mathrm{nm}$). However, one can show that under current conditions, the CARS intensity is only slightly affected by the optical density. Furthermore, careful investigation of the experimental data reveals that the minimum on the lower frequency side of the measured CEP profile does not

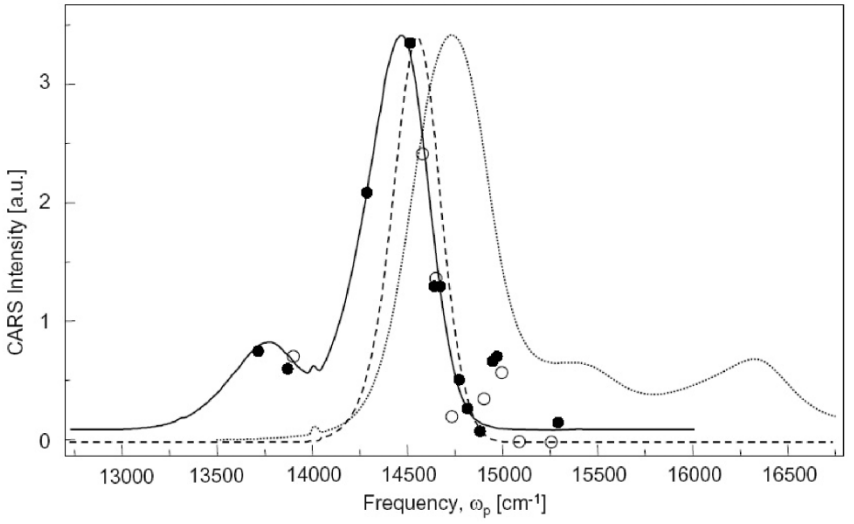

Figure 5. Intensity of CARS signal as a function of the frequency of the pump pulse (● ● ● ● / ○ ○ ○ ○). Filled and empty dots correspond to two different sets of measurements. Dashed curve shows theoretical CEP that accounts only for the strongest Raman mode ($\omega_j = 1500\,\mathrm{cm}^{-1}$). Solid curve accounts for two Raman modes ($1500\,\mathrm{cm}^{-1}$ and $700\,\mathrm{cm}^{-1}$). The Condon deviation parameter is $D = 0$ for the dashed curve and $D = 1$ for the solid curve. The absorption profile of ZnPc (- - - - -) is shown for comparison.

coincide exactly with the absorption maximum, but is slightly shifted to higher frequency. These observations render the trivial explanation unlikely.

The broken line in figure 5 shows theoretical CEP calculated according to the basic model formula (5), where we account only for the strongest ($\omega_j = 1500\,\mathrm{cm}^{-1}$) mode in the Raman spectrum. Even in this most simple case, a clear shift of the CEP is observed, and is explained by the fact that the maximum of the CEP is expected when the electronic resonance condition occurs simultaneously with the vibrational resonance.

The presence of several vibrational modes, along with the potential deviation from the Condon model, lends a possibility of a more accurate fit of the experimental CEP data. The solid curve in figure 5 was obtained by applying formula (8) to the principal vibrational mode ($1500\,\mathrm{cm}^{-1}$), along with one additional mode at $700\,\mathrm{cm}^{-1}$. Best fit was obtained with Herzberg–Teller parameter $D = 1$ for both modes. The resulting CEP was obtained by adding the two contributions, with the weight factors, $1.0\,(1500\,\mathrm{cm}^{-1})$ and $0.2\,(700\,\mathrm{cm}^{-1})$. Here we also account for the finite width of the vibration modes through introducing Gaussian factor, $\exp[-(\omega - \omega_S - \omega_j)^2/(2\Delta\omega^2)]$, where $\Delta\omega\,(700\,\mathrm{cm}^{-1}) \sim 200\,\mathrm{cm}^{-1}$ and, $\Delta\omega\,(1500\,\mathrm{cm}^{-1}) \sim 100\,\mathrm{cm}^{-1}$. In this manner, simulation allowed reproduction of all essential features of the experimental spectrum – the red shift, the width, as well as the tentative structure on the low energy side of the main peak.

The fact that a deviation from the Condon approximation can lead to an even larger shift of the CEP maximum, can be easily verified by setting $D = 1$. In this limiting case, equation (8) reduces to the product of two Φ-functions,

$$I_{\mathrm{CARS}}(\omega_\mathrm{p}) \propto |\Phi(\omega_\mathrm{p})\Phi(\omega_\mathrm{p} + \omega_j)|^2. \tag{9}$$

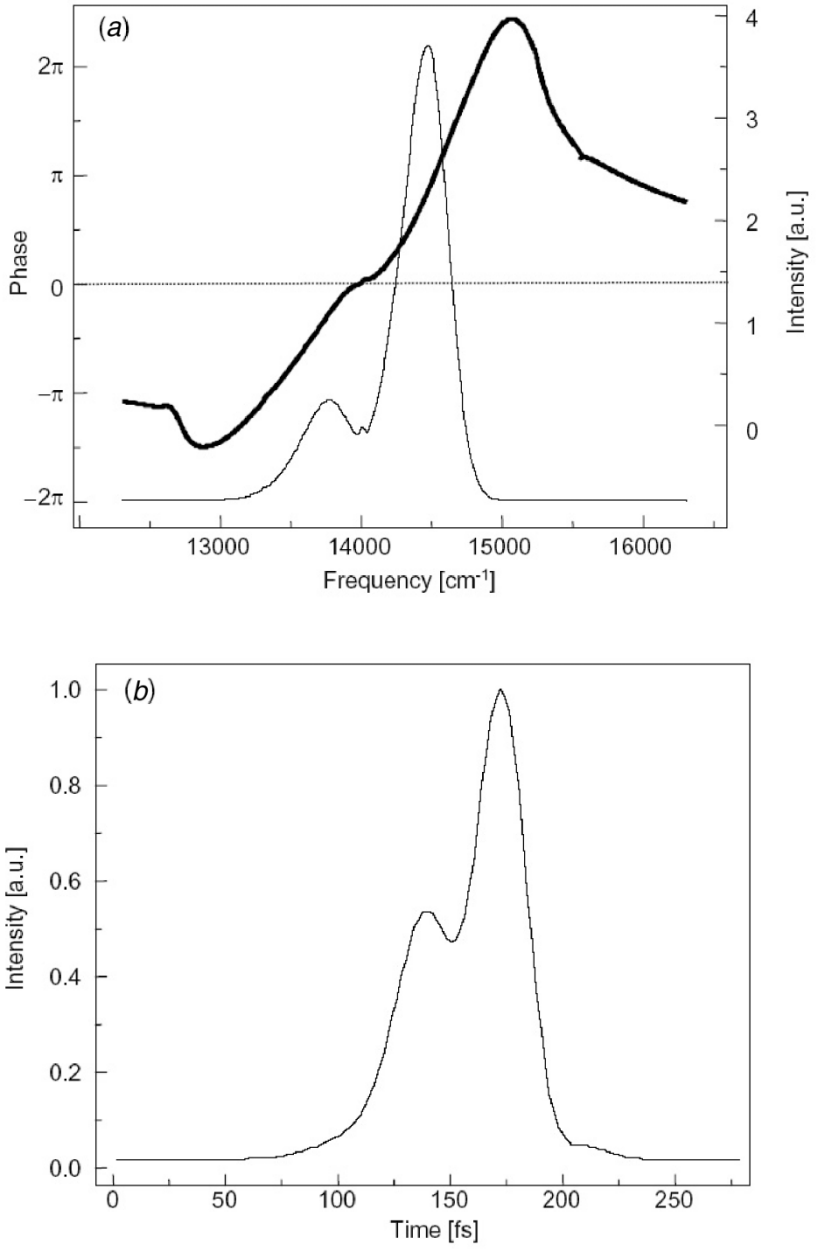

Figure 6. (*a*) Spectral phase (bold) calculated from theoretical CEP function (normal); (*b*) temporal pulse intensity profile calculated from the complex spectral amplitude.

If the characteristic vibrational frequency exceeds the characteristic width of the absorption peak, $\omega_j > \Delta\omega$, then the CEP will comprise two maxima – one at the absorption peak and the other shifted to the lower frequency by ω_j. If the opposite is the case, $\Delta\omega > \omega_j$, then the two maxima merge, shifting the overall CEP peak towards the low-frequency, by approximately one half of the vibrational frequency.

Although the last theoretical calculation agrees well with the experiment, more data is needed to finalize the analysis presented above. In particular, the Raman spectrum itself can change substantially upon resonance condition [27], which may explain the discrepancy between the measured and theoretical frequencies. Furthermore, to our knowledge, Herzberg–Teller mechanism in phthalocyanines has been previously discussed only in connection to the surface-enhanced Raman effect [28]. In our case, the $S_1 \leftarrow S_0$ electronic transition is allowed, and therefore, a more detailed consideration of the vibronic coupling is on order.

Finally, we want to point to one further possibility that the current transform theory may offer in connection with the ultrafast CARS experiments. Namely, if the goal is to obtain maximum CARS signal from a known species, then the calculated CEP profiles presented above can be viewed as an optimum spectral profile for such excitation. The corresponding spectral phase can be easily calculated either directly by using the complex index of refraction, or by applying a standard procedure, such as Hilbert phase calculation [29]. To illustrate this, figure 6(*a*) presents the Hilbert phase function obtained for the non-Condon CEP profile in figure 5. Figure 6(*b*) shows the temporal shape of a pump pulse, which corresponds to the amplitude and phase in figure 6(*a*). Using this specific pulse shape for the excitation of the CARS signal in this particular molecular species, should give a higher CARS intensity, than an equal energy, but non-optimized pulse. This last circumstance can be potentially useful for the detection of the presence of particular compounds in a mixture of species.

In conclusion, we measured coherent excitation profile of CARS signal excited with femtosecond pulses under electronic resonance conditions in ZnPc in a solid host, and without polarization discrimination of FWM background. We applied transform theory to obtain a quantitative explanation of the shift of the CEP profile towards lower frequency with respect to the absorption maximum. Our results indicate that the CEP profile measurement under the electronic resonance condition, which increases the sensitivity of the CARS signal by at least 3–4 orders of magnitude, in combination with the model calculations using transform theory, can be used as a basis for quantitative detection and identification of molecular species in ambient condensed environments.

Acknowledgements

This work was supported by AFOSR grant F49620-01-1-0406. I. Tehver thanks Estonian Science Foundation for support (Grant No. 5549). The authors thank J. Reintjes for valuable discussions concerning this paper.

References

[1] M.O. Scully, G.W. Kattawar, R.P. Lucht, *et al.*, Proc. Natl. Acad. Sci. **99** 10994–11001 (2002).
[2] G. Beadie, J. Reintjes, M. Bashkansky, *et al.*, J. Mod. Opt. **50** 2361–2368 (2003).
[3] N. Dudovich, D. Oron and Y. Silberberg, Nature **418** 512–514 (2002).
[4] A. Laubereau and W. Kaiser, Rev. Mod. Phys. **50** 607–665 (1978).
[5] A. Materny, T. Chen, M. Schmitt, *et al.*, Appl. Phys. B **71** 299–317 (2000).
[6] L.A. Rahn, L.J. Zych and P.L. Mattern, Opt. Commun. **30** 249–252 (1979).

[7] M. Schmitt, M. Heid, S. Schlucker and W. Kiefer, Biopolymers **67** 226–232 (2002).
[8] P.A. Apanasevich, V.V. Kvach and V.A. Orlovich, J. Raman Spectrosc. **20** 125–133 (1989).
[9] A. Karotki, M. Drobizhev, M. Kruk, *et al*., J. Opt. Soc. Am. B **20** 321–332 (2003); M. Drobizhev, A. Karotki, M. Kruk, *et al*., Chem. Phys. Lett. **355** 175–182 (2002).
[10] S.F. Hanna, W.D. Kulatilaka, Z. Arp, *et al*., Appl. Phys. Lett. **83** 1887–1889 (2003).
[11] V. Hizhnyakov and I. Tehver, J. Raman Spectrosc. **27** 469–474 (1996); I. Tehver, Relation between resonance scattering and absorption. Preprint F-19 of the Estonian Academy of Sciences, Tartu (1983, in Russian).
[12] V. Hizhnyakov and I. Tehver, J. Raman Spectrosc. **28** 403–410 (1997).
[13] V. Hizhnyakov and I. Tehver, Phys. Status Solidi. **21** 755–768 (1967).
[14] P.M. Champion and A.C. Albrecht, Annu. Rev. Phys. Chem. **33** 353–376 (1982).
[15] J.B. Page, in *Light Scattering in Solids* VI, edited by M. Cardona and G. Güntherodt, pp. 17–72 (Springer, Berlin, Heidelberg, New York, 1991).
[16] R.W. Boyd, *Nonlinear Optics*, 2nd Edn (Academic Press, 2003).
[17] K. Rebane, V. Hizhnyakov and I. Tehver, Proc. Estonian Acad. Sci. Phys. Math. **16** 207–232 (1967).
[18] K.K. Rebane, I.Y. Tehver and V.V. Hizhnyakov, in *Theory of Light Scattering in Condensed Matter*, edited by V.M. Agranovich and J.L. Birman, pp. 467–486 (Nauka, Moscow, 1976).
[19] M. Pfeiffer, A. Lau and W. Werncke, J. Raman Spectrosc. **15** 20–28 (1984).
[20] N. Watanabe, M. Shimizu and J. Tanaka, J. Raman Spectrosc. **13** 381–385 (1987).
[21] W.P. de Boeij, G.W. Lucassen, C. Otto, *et al*., J. Raman Spectrosc. **24** 383–396 (1993).
[22] M. Leuchs and W. Kiefer, J. Chem. Phys. **99** 6302–6307 (1993).
[23] I. Tehver, Proc. Estonian Acad. Sci. Phys. Math. **42** 329–339 (1993); V. Hizhnyakov and I. Tehver, J. Raman Spectrosc. **27** 469–474 (1996).
[24] V. Hizhnyakov and I. Tehver, J. Raman Spectrosc. **24** 653–660 (1993).
[25] A.V. Lukashin and M.D. Frank-Kamenetskii, J. Raman Spectrosc. **12** 234–237 (1982).
[26] I. Tehver, Opt. Commun. **38** 279–283 (1981).
[27] S.R. Tackley, G. Dent and W.E. Smith, Phys. Chem. Chem. Phys. **3** 1419–1426 (2001).
[28] P. Corio, J.C. Rubim and R. Aroca, Langmuir **14** 4162–4168 (1998).
[29] H. Schwoerer, D. Erni and A. Rebane, J. Opt. Soc. Am. B **12** 1083–1093 (1995).